Acoustic Klein bottle insulator

Zhenhang Pu [1,*] Hailong He [1,*] Weiyin Deng,[1] Xueqin Huang,[2] Liping Ye,[1] Jiuyang Lu,[1,†]
Manzhu Ke,[1,‡] and Zhengyou Liu[1,3,§]

[1]*Key Laboratory of Artificial Micro- and Nano-structures of Ministry of Education and School of Physics and Technology,
Wuhan University, Wuhan 430072, China*
[2]*School of Physics and Optoelectronics, South China University of Technology, Guangzhou 510640, China*
[3]*Institute for Advanced Studies, Wuhan University, Wuhan 430072, China*

Internal and crystalline symmetries play critical roles in the classification of topological materials. Recently, the crystalline symmetries are found to allow projective representations by gauge fields and bring about new topological phases, such as Möbius insulators in spinless systems. Here, we report an observation of a Klein bottle insulator (KBI) phase in phononic crystals under $\mathbb{Z}_2$ gauge fields. This intriguing insulator phase possesses, in momentum space rather than real space, a nonsymmorphic glide symmetry, under which the fundamental domain of the Brillouin zone is topologically equivalent to a Klein bottle. We exploit a bilayer structure that can be decomposed into a time-reversal-broken KBI and its time-reversal counterpart. In the acoustic KBI, a pair of edge states with a nonlocal twist are observed in experiment. All the theoretical and experimental results are in agreement and consistently validate the existence of the KBI for acoustic waves. Our work will promote the discovery of unexplored phases induced by gauge fields and offer possible applications in topological materials.

In the past decades, symmetries have resided in the core of topological material classification, which include the crystalline symmetries and the internal symmetries such as time-reversal (TR), chiral, and particle-hole symmetries [1–13]. Recently, gauge fields are attracting much attention for their promising potential in enriching symmetry algebras and generating new physics [14–22]. In systems with only positive and negative real hoppings, a specific $\mathbb{Z}_2$ gauge field has been successfully adopted to build novel topological phases in spinless systems with TR symmetry, including the Möbius insulator [23,24], mirror Chern insulator [25,26], and Kramers doublet [27]. More recently, a new Klein bottle insulator (KBI) phase is predicted in a TR-broken lattice [28]. In this KBI, the fundamental domain in momentum space is topologically equivalent to a Klein bottle, which means one pair of the domain boundaries is connected continuously while the other pair is connected antiperiodically. The Klein bottle feature stems from the underlying glide symmetry in momentum space, and more importantly, implies a pair of nonlocally related edge states in this TR-broken KBI beyond the conventional bulk-edge correspondence.

However, realizing such a TR-broken KBI is not easily accessible in real systems, considering the challenge in breaking the TR symmetry, especially for scalar acoustic waves [29–38]. Fortunately, the high tunability of phononic crystals (PCs) makes it feasible to introduce additional degrees of freedom. A natural question arises: is it possible to achieve TR-broken KBIs in PCs by introducing additional degrees of freedom yet retain the TR symmetry of the whole system? The spinless mirror Chern insulator may spark inspiration, where a bilayer structure is divided into two Chern insulators with opposite Chern numbers [19,25,26]. With the additional layer of degrees of freedom, the dispersions with glide and fractional translation symmetries in KBIs can be visualized in experiments. Note that the glide symmetry, as a nonsymmorphic symmetry that originally exists only in real space, is now extended to momentum space in KBIs, giving rise to the Klein bottle topology.

In this Letter, we report an observation of acoustic KBI, which comes from a bilayer structure connected with positive and negative hoppings. The construction of the acoustic KBI is based on a well-established lattice model with specific $\mathbb{Z}_2$ gauge fields, i.e., hoppings are real with amplitudes taking a $\pm$ sign. The imposed gauge fields decompose the bilayer lattice into a KBI and its TR counterpart. Note that the TR symmetry in each KBI is broken but is retained when the other KBI is involved. With the model implemented in PCs, the acoustic KBI is verified by the glide symmetry in momentum space and the fractional translations for the in-gap edge state dispersions. Our findings evidence the Klein bottle feature embedding in the Brillouin zone (BZ) and broaden perspectives to topological phases in terms of gauge fields.

To construct the KBI, we start with a lattice model with periodicity along the x and y directions and unity lattice constants, as shown in Fig. 1(a). It is a bilayer lattice whose Hamiltonian has the form $H_{\mathrm{B}} = \begin{bmatrix} H_0 & C_0 \\ C_0^{\dagger} & H_0 \end{bmatrix}$, where H_0 describes one of the two identical layers, and C_0 and its Hermitian conjugate $C_0^{\dagger}$ represent the couplings between them [39]. The orbitals denoted by cyan and yellow spheres have opposite on-site energies, while the positive and negative

_____

*These authors contributed equally to this work.
†Corresponding author: jylu@whu.edu.cn
‡Corresponding author: mzke@whu.edu.cn
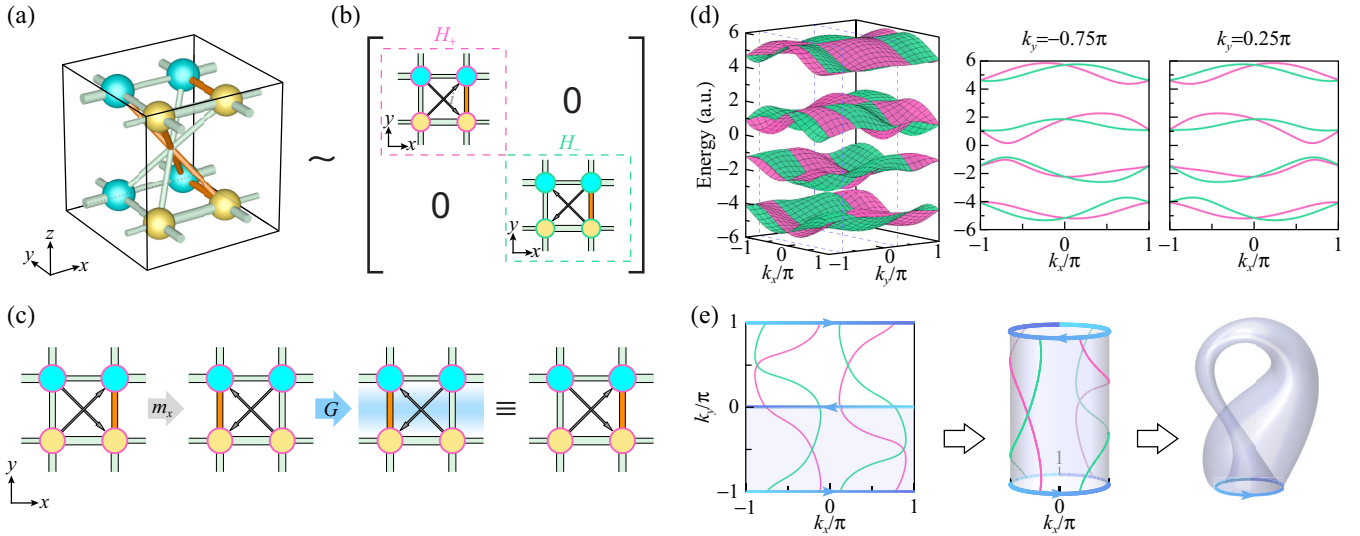§Corresponding author: zyliu@whu.edu.cn

FIG. 1. Construction of KBIs in a bilayer lattice. (a) The unit cell of the bilayer lattice, which contains eight sites connected by positive and negative hoppings (denoted by green and orange tubes). (b) Two monolayer lattices arising from the decomposition of the bilayer one. The negative and positive hoppings enclose plaquettes with π flux. The imaginary hoppings originating from the interlayer ones are denoted by arrows. (c) Illustration of the gauge-modified mirror symmetry of the monolayer lattice, which is a combination of the mirror symmetry m_x and the gauge transformation G. G imposes an additional "–" sign to hoppings in the shaded region in the third panel. (d) Left panel: 3D view of the bulk band structure. Middle and right panels: the bulk bands at $k_y = -0.75\pi$ and 0.25π, respectively. (e) Schematics of the Klein bottle structure embedding in the BZ. The magenta and green bands or curves in (d) and (e) are calculated for $H_\pm$ with all the parameters provided in [39].

hoppings are distinguished by green and orange tubes, respectively. Due to the presence of negative hoppings (orange tubes), the mirror symmetries along the x and z directions are broken simultaneously. And to expose the specific band structures in KBI, the hopping parameters are chosen to further reduce the symmetries of the lattice [39].

Under the gauge fields, the above bilayer lattice can decompose into a pair of TR-related KBIs, as illustrated in Fig. 1(b). The decomposition can be performed by a unitary transformation $U = \frac{1}{\sqrt{2}}\begin{bmatrix} 1 & i \\ 1 & -i \end{bmatrix} \otimes I_4$ with I_4 being an identity matrix of dimension four and $\otimes$ denoting the Kronecker product [40]. Through the unitary transformation, the basis states in the upper and lower layers are mixed as $\psi_\pm = (\psi_{\text{low}} \pm i\psi_{\text{up}})/\sqrt{2}$. One thus obtains a block-diagonal Hamiltonian $UH_B U^{-1} = H_+ \oplus H_-$, where $H_\pm = H_0 \mp iC_0$ correspond to the Hamiltonians living in monolayer subspaces spanned by the new basis [denoted by the magenta and green circles in Fig. 1(b)]. The $H_\pm$ exactly represent two KBIs, whose on-site energies (denoted by cyan and yellow dots) and the monolayer hoppings (denoted by green and orange rods) remain unchanged with respect to those in Fig. 1(a). And in addition, for the existence of the $\mathbb{Z}_2$ gauge fields, the original real interlayer hopping terms represented by C_0 in Fig. 1(a) have been switched to the imaginary monolayer ones $\mp iC_0$ denoted by gray arrows in Fig. 1(b) [19,25,26]. Thus, for either one monolayer Hamiltonian, H_+ or H_-, the TR symmetry is broken, while it restores when both are involved. This leads to the asymmetric but TR-related band structures for the monolayer Hamiltonians.

Now we unveil the gauge-field-induced glide symmetry in momentum space, a unique feature of KBI [28]. Taking the

monolayer Hamiltonian H_+ as an example, its TR counterpart can be analyzed similarly. As illustrated in Fig. 1(c), through a mirror symmetry normal to the x direction, i.e., $m_x : x \to -x$, the π flux in each plaquette (enclosed by one negative and three positive hoppings) remains while the gauge connection changes. To restore the change in configuration, an additional gauge transformation $G = (+I_2) \otimes (-I_2)$ is required, and the composited symmetry is the gauge-modified mirror $M_x = Gm_x = \sigma_z \otimes \sigma_x$ with σ denoting the Pauli matrix. In such enriched symmetry algebra, the conventional commutation between the mirror and the lattice translation along the y direction (denoted as L_y) is modified to an anticommutation relation $\{M_x, L_y\} = 0$ [28]. Represented in momentum space and recalling that $L_y = e^{ik_y}$, the anticommutation relation requires $M_x e^{ik_y} M_x^{-1} = -e^{ik_y} = e^{i(k_y+\pi)}$, that is, a 1/2 fractional translation is associated to M_x. As such, a glide symmetry is generated in momentum space, which acts on the monolayer Hamiltonians as $M_x H_\pm(k_x, k_y) M_x^{-1} = H_\pm(-k_x, k_y + \pi)$. Note that it is possible to design the physical mirror involving the layer degree of freedom as $M_x \oplus M_x$, which commutes with the aforementioned unitary transformation U.

The glide symmetry in momentum space can be visually reflected by the bulk band structures in Fig. 1(d), i.e., $\epsilon_\pm(k_x, k_y) = \epsilon_\pm(-k_x, k_y + \pi)$ with $\epsilon_\pm$ being the eigenvalues of $H_\pm$. In the left panel, the blue dashed rectangles outline two slices of the bulk bands with a distance of π in k_y [$\epsilon_\pm(k_x, -0.75\pi)$ and $\epsilon_\pm(k_x, 0.25\pi)$], which are respectively plotted in the middle and right panels. One can see that the band structure at $k_y = 0.25\pi$ is identical to that at $k_y = -0.75\pi$ via inversing one of the k_x directions. In other words, these two band structures are oppositely

oriented in the presence of the glide symmetry in momentum space.

This feature exactly gives the Klein bottle structure embedding in the BZ. More intuitively, we focus on isoenergy contours in the left panel of Fig. 1(e), where the magenta and green curves respectively correspond to $\epsilon_{\pm} = 1.5$ and they are TR-related as expected, i.e., $\epsilon_{+}(k_x, k_y) = \epsilon_{-}(-k_x, -k_y)$. Remarkably, each of them respects the glide symmetry along the k_y direction. Because of the glide symmetry, the fundamental domain in momentum space, denoted as the shaded region in Fig. 1(e), is reduced to half of the BZ, that is, the other half can be generated under the action of the glide symmetry. Although only half of the BZ is involved, the fundamental domain is competent to capture the topological information of the system [28]. As illustrated in the middle and right panels of Fig. 1(e), the fundamental domain is equivalent to a cylinder after rolling and gluing the oriented boundaries, and can further be deformed to a Klein bottle by gluing the oppositely oriented boundaries (denoted by blue curves with arrows). Note that the choice of the fundamental domain is not unique because the glide symmetry, different to the conventional space group symmetries, is a free operator without invariant symmetry elements in momentum space.

The topology of the KBIs can be determined by the topological invariant ν, denoting the odd or even times for the Berry phase γ crossing π as k_y runs from $-\pi$ to 0. Specifically, even times crossing corresponds to a trivial phase $\nu = 0$, while odd times corresponds to a nontrivial $\nu = 1$ that protects the emergence of in-gap edge states [28]. In the nontrivial phase, in-gap states are ensured by a Berry phase of π for a specific k_y-fixed one-dimensional subsystem, and then the edge bands can be formed due to the continuity of the energy bands. When inducing boundary potentials, the edge states can be moved in spectra. In our case, both $H_{\pm}$ of KBIs are nontrivial and possess $\nu = 0, 1, 0,$ and 1 for the four isolated bands, implying the existence of in-gap edge states. In contrast to the conventional crystalline insulators with symmetry-protected edge states hosted on symmetry-preserving edges, the edge states in KBI can exist on the symmetry-breaking edges. Furthermore, with the M_x-related edges along the y direction, the Klein bottle nature can result in a pair of edge states with a nonlocal twist, whose band structures are related by a 1/2 fractional translation of π in k_y [39].

To implement the acoustic KBI, we construct a bilayer PC sample with a set of cavities connected by elaborate tubes, as shown in Fig. 2(a). The sample is fabricated by three-dimensional (3D) printing and contains 26×32 unit cells (along the x and y directions) with the sample thickness of 50.8 mm in the z direction. Figure 2(b) depicts the schematics of the unit cell with the lattice constants $a_0 = 48.0$ mm and $b_0 = 21.0$ mm. The colored cavities, $\pm 45°$ tilted in the XZ plane, are separated by the distances of $a_0/2$ and $b_0/2$ in the x and y directions. The cavities are also related by a fourfold rotational axis along the y direction locating at the center of the unit cell. The shapes of the cyan and yellow cavities are different in height, and their dipolar modes are chosen to map orbitals with different on-site energies. When connecting the cavities according to the acoustic field distribution of the dipolar mode, positive and negative hoppings are achieved
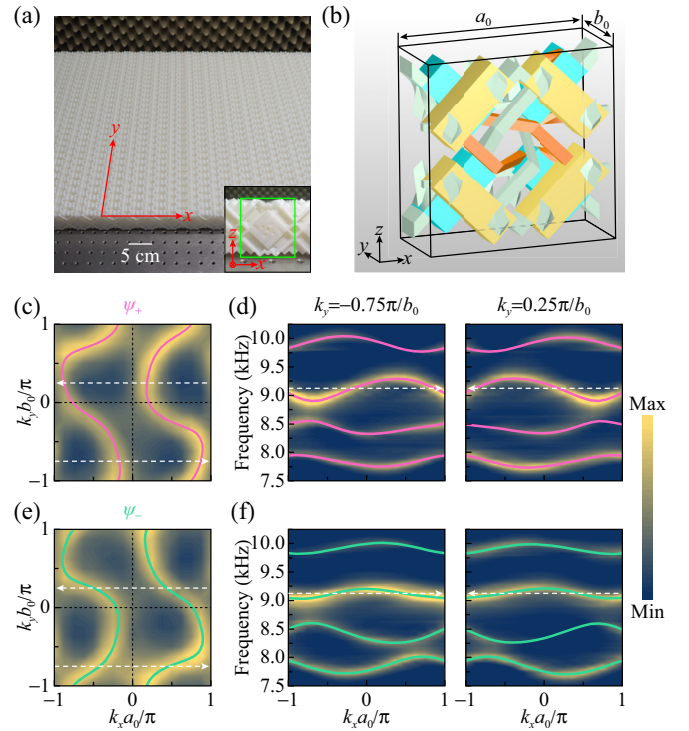

FIG. 2. Observation of the acoustic KBI. (a) A photo of the real PC. The inset shows the side view and the unit cell is boxed in green. (b) Schematics of the unit cell. All the colored regions are filled with air and bounded with hard boundaries. (c) The isofrequency contours of ψ_+ at the frequency of 9.12 kHz. (d) Left and right panels: the bulk dispersions of ψ_+ at $k_y = -0.75\pi/b_0$ and $0.25\pi/b_0$, respectively, with the route denoted by the white dashed lines in (c). The white dashed lines in (d) label the frequency of 9.12 kHz. (e) and (f) The same as (c) and (d) but for ψ_-. In (c)–(f), the colormaps and the solid lines correspond to the measured and simulated results, respectively.

[41–44]. The tubes introducing positive and negative hoppings are colored in green and orange in Fig. 2(b), respectively. The intralayer tubes are designed to respect a mirror symmetry about the XY plane to equalize the hopping strengths within the upper and lower layers; the chiral interlayer tubes respect a fourfold rotational symmetry. Although unavoidable long-range couplings slightly affect the symmetry of our acoustic system [23,24], such designed PC can reproduce to a large extent the band structures and the topological properties of the ideal lattice model [39].

We now observe the dispersions for the acoustic KBIs in experiment. A broadband point sound source is located at the center of the upper layer to stimulate the pressure fields in both layers ψ_{low} and ψ_{up}. To observe the acoustic KBIs, one needs to obtain the states in the monolayer subspaces as in the lattice model, which hybrids ψ_{low} and ψ_{up} as $\psi_{\pm} = (\psi_{\text{low}} \pm i\psi_{\text{up}})/\sqrt{2}$. These subspace-resolved fields $\psi_{\pm}$ can be further Fourier transformed into momentum space. Following this procedure, the isofrequency contours of $\psi_{\pm}$ are obtained, as displayed in Figs. 2(c) and 2(e). Each set of contours respect a glide symmetry along the k_y direction, unambiguously identifying the existence of the Klein bottle. One can also see that the two sets of contours are TR counterparts as they are
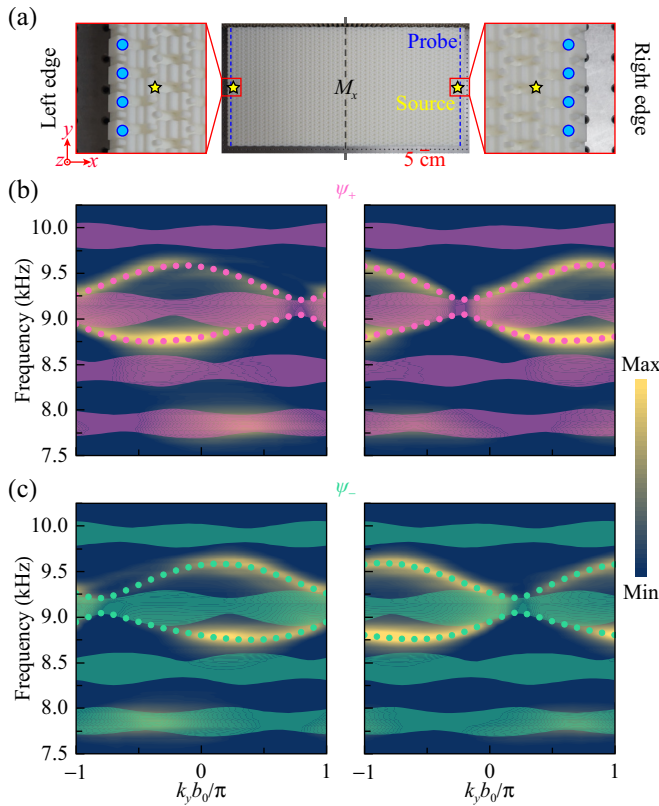
FIG. 3. Observation of the edge states with a nonlocal twist. (a) Experiment for edge states observation. (b) Edge dispersions of ψ_+. The colormap in the left (right) panel represents the measured result at the left (right) edge. The shaded regions and the colored circles denote the simulated bulk and edge states, respectively. (c) The same as (b) but for ψ_-.

with the measurement positions denoted by the circles in the enlarged insets]. Following the procedure used in the bulk dispersion observation, we recombine the measured edge fields in both layers to give the subspace-resolved fields and obtain the corresponding edge dispersions after performing Fourier transformations. As displayed by the colormaps in Figs. 3(b) and 3(c), the edge dispersions of $\psi_\pm$ are clearly observed, which are in good agreement with the simulated results (colored circles). For each KBI, the edge dispersion at one edge of the PC can translate to the other edge through the 1/2 fractional translation of π/b_0 along the k_y direction as predicted. That is, only the projected BZ in $[-\pi/b_0, 0)$ is independent and the rest can be repeated by the fractional translation. For the two TR-related KBIs, the dispersions of ψ_+ and ψ_- on the same edge are oppositely oriented with respect to the k_y direction. Note that the dispersion of the whole bilayer structure involves the dispersions of both ψ_+ and ψ_-, thereby doubling the propagating channels of the edge states [45–47].

In conclusion, we have observed the acoustic KBIs, unveiling the Klein bottle topology and nonsymmorphic glide symmetry in momentum space. Recently, several individual works also reported the momentum-space glide symmetries in monolayer and 3D PCs [48–50]. In our work, the bilayer PC is carefully designed so that a pair of TR-broken KBIs is formed. In each acoustic TR-broken KBI, edge states with a nonlocal twist emerge in the band gaps, which, beyond the conventional bulk-edge correspondence, are required by the geometrical constraints of the Klein bottle. It is noted that the $\mathbb{Z}_2$ gauge fields are important to the constructions of the TR-broken KBI and the underlying nonsymmorphic glide symmetry in momentum space. Our work expands the scope of realizing novel topological phases from the temporal and spatial symmetries to the fields of gauge symmetries [17,20], which is broadly applicable to a variety of systems such as mechanical [29,33], electric circuit [51–53], photonic [30,31], and cold atom systems [54]. In addition, our work shows the feasibility of classical wave manipulation using mechanisms with gauge fields, and the successful implementation of acoustic KBIs paves the way towards elastic wave systems, which may have broader application potential [55–57].

connected by inversion with respect to the TR-invariant BZ center. To further verify the Klein bottle nature, we extract the dispersions of $\psi_\pm$, as shown in Figs. 2(d) and 2(f). Taking the ψ_+ as an example, the dispersions at $k_y = -0.75\pi/b_0$ and $0.25\pi/b_0$ [corresponding respectively to the left and right panels of Fig. 2(d)] are oppositely oriented as expected. The dispersions of ψ_- shown in Fig. 2(f) can be similarly analyzed.

Finally, we demonstrate the edge states of the acoustic KBI, whose dispersions are related by 1/2 fractional translations of π/b_0 in k_y. As illustrated in Fig. 3(a), the left and right edges of the PC sample are connected by M_x. To excite the edge acoustic fields, a point source is inserted into the center cavity of the left or right edge in the upper layer, as labeled by the yellow stars. The signals in both layers are recorded from the edge cavities [blue dashed lines in Fig. 3(a)

[1] M. Z. Hasan and C. L. Kane, *Colloquium*: Topological insulators, Rev. Mod. Phys. **82**, 3045 (2010).

[2] S. Ryu, A. P. Schnyder, A. Furusaki, and A. W. W. Ludwig, Topological insulators and superconductors: Tenfold way and dimensional hierarchy, New J. Phys. **12**, 065010 (2010).

[3] X.-L. Qi and S.-C. Zhang, Topological insulators and superconductors, Rev. Mod. Phys. **83**, 1057 (2011).

[4] A. Bansil, H. Lin, and T. Das, *Colloquium*: Topological band theory, Rev. Mod. Phys. **88**, 021004 (2016).

[5] C.-K. Chiu, Classification of topological quantum matter with symmetries, Rev. Mod. Phys. **88**, 035005 (2016).

[6] N. P. Armitage, E. J. Mele, and A. Vishwanath, Weyl and Dirac semimetals in three-dimensional solids, Rev. Mod. Phys. **90**, 015001 (2018).

[7] T. Zhang, Y. Jiang, Z. Song, H. Huang, Y. He, Z. Fang, H. Weng, and C. Fang, Catalogue of topological electronic materials, Nature (London) **566**, 475 (2019).

[8] M. G. Vergniory, L. Elcoro, C. Felser, N. Regnault, B. A. Bernevig, and Z. Wang, A complete catalogue of high-quality topological materials, Nature (London) **566**, 480 (2019).

[9] F. Tang, H. C. Po, A. Vishwanath, and X. Wan, Comprehensive search for topological materials using symmetry indicators, Nature (London) **566**, 486 (2019).

[10] B. Q. Lv, T. Qian, and H. Ding, Experimental perspective on three-dimensional topological semimetals, Rev. Mod. Phys. **93**, 025002 (2021).

[11] M. G. Vergniory, B. J. Wieder, L. Elcoro, S. S. P. Parkin, C. Felser, B. A. Bernevig, and N. Regnault, All topological bands of all nonmagnetic stoichiometric materials, Science **376**, eabg9094 (2022).

[12] B. J. Wieder, B. Bradlyn, J. Cano, Z. Wang, M. G. Vergniory, L. Elcoro, A. A. Soluyanov, C. Felser, T. Neupert, N. Regnault *et al.*, Topological materials discovery from crystal symmetry, Nat. Rev. Mater. **7**, 196 (2022).

[13] B. A. Bernevig, C. Felser, and H. Beidenkopf, Progress and prospects in magnetic topological materials, Nature (London) **603**, 41 (2022).

[14] X.-G. Wen, Quantum orders and symmetric spin liquids, Phys. Rev. B **65**, 165113 (2002).

[15] L. Messio, C. Lhuillier, and G. Misguich, Time reversal symmetry breaking chiral spin liquids: Projective symmetry group approach of bosonic mean-field theories, Phys. Rev. B **87**, 125127 (2013).

[16] S. Bieri, C. Lhuillier, and L. Messio, Projective symmetry group classification of chiral spin liquids, Phys. Rev. B **93**, 094437 (2016).

[17] Y. X. Zhao, Y.-X. Huang, and S. A. Yang, $\mathbb{Z}_2$-projective translational symmetry protected topological phases, Phys. Rev. B **102**, 161117(R) (2020).

[18] Y. X. Zhao, C. Chen, X. L. Sheng, and S. A. Yang, Switching spinless and spinful topological phases with projective *PT* symmetry, Phys. Rev. Lett. **126**, 196402 (2021).

[19] L. B. Shao, Z. Y. Chen, K. Wang, S. A. Yang, and Y. X. Zhao, Spinless mirror Chern insulator from projective symmetry algebra, Phys. Rev. B **108**, 205126 (2023).

[20] Z. Y. Chen, Z. Zhang, S. A. Yang, and Y. X. Zhao, Classification of time-reversal-invariant crystals with gauge structures, Nat. Commun. **14**, 743 (2023).

[21] H. Xue, Z. Y. Chen, Z. Cheng, J. X. Dai, Y. Long, Y. X. Zhao, and B. Zhang, Stiefel-Whitney topological charges in a three-dimensional acoustic nodal-line crystal, Nat. Commun. **14**, 4563 (2023).

[22] X. Xiang, X. Ni, F. Gao, X. Wu, Z. Chen, Y.-G. Peng, and X.-F. Zhu, Demonstration of acoustic high-order Stiefel-Whitney semimetal in bilayer graphene sonic crystals, arXiv:2304.12735.

[23] H. Xue, Z. Wang, Y. X. Huang, Z. Cheng, L. Yu, Y. X. Foo, Y. X. Zhao, S. A. Yang, and B. Zhang, Projectively enriched symmetry and topology in acoustic crystals, Phys. Rev. Lett. **128**, 116802 (2022).

[24] T. Li, J. Du, Q. Zhang, Y. Li, X. Fan, F. Zhang, and C. Qiu, Acoustic Möbius insulators from projective symmetry, Phys. Rev. Lett. **128**, 116803 (2022).

[25] H. Xue, D. Jia, Y. Ge, Y.-j. Guan, Q. Wang, S.-q. Yuan, H.-x. Sun, Y. D. Chong, and B. Zhang, Observation of dislocation-induced topological modes in a three-dimensional acoustic topological insulator, Phys. Rev. Lett. **127**, 214301 (2021).

[26] T. Li, L. Liu, Q. Zhang, and C. Qiu, Acoustic realization of projective mirror Chern insulators, Commun. Phys. **6**, 268 (2023).

[27] Y. Meng, S. Lin, B.-J. Shi, B. Wei, L. Yang, B. Yan, Z. Zhu, X. Xi, Y. Wang, Y. Ge *et al.*, Spinful topological phases in acoustic crystals with projective *PT* symmetry, Phys. Rev. Lett. **130**, 026101 (2023).

[28] Z. Y. Chen, S. A. Yang, and Y. X. Zhao, Brillouin Klein bottle from artificial gauge fields, Nat. Commun. **13**, 2215 (2022).

[29] S. D. Huber, Topological mechanics, Nat. Phys. **12**, 621 (2016).

[30] L. Lu, J. D. Joannopoulos, and M. Soljačić, Topological states in photonic systems, Nat. Phys. **12**, 626 (2016).

[31] T. Ozawa, H. M. Price, A. Amo, N. Goldman, M. Hafezi, L. Lu, M. C. Rechtsman, D. Schuster, J. Simon, O. Zilberberg *et al.*, Topological photonics, Rev. Mod. Phys. **91**, 015006 (2019).

[32] X. Zhang, M. Xiao, Y. Cheng, M.-H. Lu, and J. Christensen, Topological sound, Commun. Phys. **1**, 97 (2018).

[33] G. Ma, M. Xiao, and C. T. Chan, Topological phases in acoustic and mechanical systems, Nat. Rev. Phys. **1**, 281 (2019).

[34] B. Xie, H.-X. Wang, X. Zhang, P. Zhan, J.-H. Jiang, M. Lu, and Y. Chen, Higher-order band topology, Nat. Rev. Phys. **3**, 520 (2021).

[35] H. Xue, Y. Yang, and B. Zhang, Topological acoustics, Nat. Rev. Mater. **7**, 974 (2022).

[36] R. Fleury, D. L. Sounas, C. F. Sieck, M. R. Haberman, and A. Alu, Sound isolation and giant linear nonreciprocity in a compact acoustic circulator, Science **343**, 516 (2014).

[37] Z. Yang, F. Gao, X. Shi, X. Lin, Z. Gao, Y. Chong, and B. Zhang, Topological acoustics, Phys. Rev. Lett. **114**, 114301 (2015).

[38] Y. Ding, Y. Peng, Y. Zhu, X. Fan, J. Yang, B. Liang, X. Zhu, X. Wan, and J. Cheng, Experimental demonstration of acoustic Chern insulators, Phys. Rev. Lett. **122**, 014302 (2019).

[39] See Supplemental Material at http://link.aps.org/supplemental/10.1103/PhysRevB.108.L220101 for more discussions of the theoretical model, geometric details of the phononic crystal, and the simulated and experimental methods.

[40] R. Süsstrunk and S. D. Huber, Observation of phononic helical edge states in a mechanical topological insulator, Science **349**, 47 (2015).

[41] Y. Qi, C. Qiu, M. Xiao, H. He, M. Ke, and Z. Liu, Acoustic realization of quadrupole topological insulators, Phys. Rev. Lett. **124**, 206601 (2020).

[42] X. Ni, M. Li, M. Weiner, A. Alu, and A. B. Khanikaev, Demonstration of a quantized acoustic octupole topological insulator, Nat. Commun. **11**, 2108 (2020).

[43] H. Xue, Y. Ge, H. X. Sun, Q. Wang, D. Jia, Y. J. Guan, S. Q. Yuan, Y. Chong, and B. Zhang, Observation of an acoustic octupole topological insulator, Nat. Commun. **11**, 2442 (2020).

[44] Z. Pu, H. He, L. Luo, Q. Ma, L. Ye, M. Ke, and Z. Liu, Acoustic higher-order Weyl semimetal with bound hinge states in the continuum, Phys. Rev. Lett. **130**, 116103 (2023).

[45] S. A. Skirlo, L. Lu, and M. Soljačić, Multimode one-way waveguides of large Chern numbers, Phys. Rev. Lett. **113**, 113904 (2014).

[46] S. A. Skirlo, L. Lu, Y. Igarashi, Q. Yan, J. Joannopoulos, and M. Soljačić, Experimental observation of large Chern numbers in photonic crystals, Phys. Rev. Lett. **115**, 253901 (2015).

[47] C. Vega, D. Porras, and A. González-Tudela, Topological multimode waveguide QED, Phys. Rev. Res. **5**, 023031 (2023).

[48] Y. Wang, C. Zhang, Z. Chen, B. Liang, Y. Zhao, and J. Cheng, Chess-board acoustic crystals with momentum-space nonsymmorphic symmetries, arXiv:2305.07174.

[49] Z. Zhu, L. Yang, J. Wu, Y. Meng, X. Xi, B. Yan, J. Chen, J. Lu, X. Huang, W. Deng *et al.*, Brillouin Klein space and half-turn space in three-dimensional acoustic crystals, arXiv:2305.08450.

[50] Y.-L. Tao, M. Yan, M. Peng, Q. Wei, Z. Cui, S. A. Yang, G. Chen, and Y. Xu, Higher-order Klein bottle topological insulator in three-dimensional acoustic crystals, arXiv:2305.09174.

[51] S. Imhof, C. Berger, F. Bayer, J. Brehm, L. W. Molenkamp, T. Kiessling, F. Schindler, C. H. Lee, M. Greiter, T. Neupert *et al.*, Topolectrical-circuit realization of topological corner modes, Nat. Phys. **14**, 925 (2018).

[52] D. Zou, T. Chen, W. He, J. Bao, C. H. Lee, H. Sun, and X. Zhang, Observation of hybrid higher-order skin-topological effect in non-Hermitian topolectrical circuits, Nat. Commun. **12**, 7201 (2021).

[53] J. Wu, Z. Wang, Y. Biao, F. Fei, S. Zhang, Z. Yin, Y. Hu, Z. Song, T. Wu, F. Song *et al.*, Non-Abelian gauge fields in circuit systems, Nat. Electron. **5**, 635 (2022).

[54] N. R. Cooper, J. Dalibard, and I. B. Spielman, Topological bands for ultracold atoms, Rev. Mod. Phys. **91**, 015005 (2019).

[55] M. Serra-Garcia, V. Peri, R. Süsstrunk, O. R. Bilal, T. Larsen, L. G. Villanueva, and S. D. Huber, Observation of a phononic quadrupole topological insulator, Nature (London) **555**, 342 (2018).

[56] M. Yan, J. Lu, F. Li, W. Deng, X. Huang, J. Ma, and Z. Liu, On-chip valley topological materials for elastic wave manipulation, Nat. Mater. **17**, 993 (2018).

[57] Q. Zhang, D. Lee, L. Zheng, X. Ma, S. I. Meyer, H. Ye, Z. Gong, B. Zhen, K. Lai *et al.*, Gigahertz topological valley Hall effect in nanoelectromechanical phononic crystals, Nat. Electron. **5**, 157 (2022).